Rheological Analysis and Measurement of Neutrophil Indentation

E. B. Lomakina,* C. M. Spillmann,† M. R. King,‡ and R. E. Waugh‡
*Department of Pharmacology and Physiology, †Department of Biochemistry and Biophysics, and ‡Department of Biomedical Engineering, University of Rochester, Rochester, New York

ABSTRACT Aspects of neutrophil mechanical behavior relevant to the formation of adhesive contacts were assessed by measuring the dependence of the contact area between the cell and a spherical substrate under controlled loading. Micropipettes were used to bring neutrophils into contact with spherical beads under known forces, and the corresponding contact area was measured over time. The neutrophil was modeled as a viscous liquid drop with a constant cortical tension. Both the equilibrium state and the dynamics of the approach to equilibrium were examined. The equilibrium contact area increased monotonically with force in a manner consistent with a cell cortical tension of 16–24 pN/μm. The dynamic response matched predictions based on a model of the cell as a growing drop using published values for the effective viscosity of the cell. The contact pressure between the cell and substrate at equilibrium is predicted to depend on the curvature of the contacting substrate, but to be independent of the impingement force. The approach to equilibrium was rapid, such that the time-averaged stress for a two-second impingement was within 20% of the equilibrium value. These results have implications for the role of mechanical force in the formation of adhesive contacts.

INTRODUCTION

Deformation of neutrophils in response to external forces is intrinsic to their function as circulating cells. It is important not only during their passage through small apertures in the circulation, but also as they flatten and deform during interaction and adhesion with the endothelium. Experiments testing passive neutrophil deformation have led to the development of mechanical models that approximate the cellular response to applied forces. An early report based on small deformations of the cell into a micropipette used the model of a standard viscoelastic solid to describe cell behavior (Schmid-Schonbein et al., 1981). Subsequently, observations of large cellular deformations demonstrated that neutrophil behavior is fundamentally fluid-like: cells deform continuously into micropipettes in response to constant loads (Evans and Kukan, 1984). These observations led to the model of the cell as a viscous fluid with a constant cortical tension, the so-called *liquid-drop model* (Evans and Kukan, 1984; Evans and Yeung, 1989; Needham and Hochmuth, 1990). In the simplest form, the neutrophil cytoplasm is modeled as a Newtonian fluid. A thorough examination of cellular behavior reveals that the behavior is more complex than this, and a number of refinements to the basic liquid-drop model have been proposed. These include models of the cell in which there is a significant surface viscosity (Evans and Yeung, 1989; Yeung and Evans, 1989; Drury and Dembo, 2001; Herant et al., 2003), two-phase flow (Herant et al., 2003), inclusion of a transient elastic component (Dong and Skalak, 1992), and recognition that the cellular viscosity decreases with increasing rate of deformation (Tsai et al., 1993; Drury and Dembo, 2001). Nevertheless, the simple Newtonian drop model captures the essential behavior of the cell.

Neutrophil deformation can have a significant influence on the adhesion of cells to substrates under hydrodynamic shear. Previously, an approximate, two-dimensional analysis of adherent deformable bodies in shear flow has been used to examine the effects of deformation on adhesion in shear flow (Dong et al., 1999; Lei et al., 1999). Leukocyte deformation can enhance adhesion in at least three ways. First, after initial contact and adhesion, hydrodynamic forces acting on the cell increase the area of contact, increasing the number of receptors and ligands available for bond formation. Second, the lengthening of the contact zone increases the moment arm over which bond forces at the periphery act, reducing the magnitude of the force on bonds at the rear of the cell acting to counteract hydrodynamic forces working to detach the cell from the surface. Third, cell flattening reduces the overall hydrodynamic drag force exerted by the external flow on the cell surface (Dimitrakopoulos and Higdon, 1998; Lei et al., 1999). These three effects together add significantly to the stability of adhesion and enhance the effective recruitment of cells from the vasculature.

In addition to these macroscopic effects on adhesion in shear flow, mechanical forces may affect adhesion via alterations of the surface microtopography of the cell membrane in the contact zone. The microvilli that cover the neutrophil surface limit the proportion of the cell membrane that may come in molecularly close contact with an opposing surface (Williams et al., 2001). This in turn may reduce the accessibility of adhesion molecules for bond formation with the substrate. This effect may be enhanced (or mitigated)

Submitted July 22, 2003, and accepted for publication September 1, 2004.

E. B. Lomakina and C. M. Spillmann contributed equally to the work.

Address reprint requests to Richard E. Waugh, Dept. of Biomedical Engineering, University of Rochester, Medical Center Box 639, 601 Elmwood Ave., Rochester, NY 14642. Tel.: 585-275-3768; Fax: 585-273-4746; E-mail: waugh@seas.rochester.edu.

0006-3495/04/12/4246/13 $2.00

doi: 10.1529/biophysj.103.031765

by the nonuniform distribution of adhesion molecules over the cell surface. Ultrastructural evidence indicates that the distribution of the major adhesion molecules on the neutrophil surface is, in fact, nonuniform. A neutrophil receptor known to mediate cell rolling, L-selectin, is primarily clustered on the tips of microvilli as shown by immunogold labeling (Erlandsen et al., 1993; Bruehl et al., 1996). In contrast, the principal integrin receptors on the neutrophil surface (LFA-1 and Mac-1) appear to be randomly distributed on the non-villus cell body (Erlandsen et al., 1993; Fernandez-Segura et al., 1996). To evaluate the extent that stresses between the cell and substrate may affect the microtopography of the contact zone, it is important to know how the contact pressure (which is directly related to the mean force per microvillus in the contact region) changes under different loading conditions.

In this report we assess aspects of neutrophil mechanical behavior relevant to the formation of adhesive contacts between neutrophils and an artificial surface under well-controlled conditions. Micropipettes were used to make contact between neutrophils and beads with different applied forces, and the time-course of the approach to equilibrium was observed. This behavior is compared to analytical predictions based on published mechanical models of the neutrophil. In a companion report (Spillmann et al., 2004), the implications of this behavior are used as a basis for understanding the dependence of adhesion on impingement force.

ANALYSIS

Equilibrium

We first consider the equilibrium case of a passive neutrophil and a rigid bead touched together under a constant axial force. This interaction results in deformation of the cell by the bead and formation of a measurable area of contact between the two surfaces. To determine the equilibrium relationship between contact area and force we treated the cell as a viscous liquid drop with a constant uniform cortical tension, neglecting any contributions to the deformation due to bending resistance of the cell cortex. In keeping with the model of the cell as a liquid drop, the interior pressure at equilibrium is presumed to be uniform. The geometry of the interaction is depicted in Fig. 1.

The macroscopic contact area, A_{mac}, between the cell and bead is related to the radius of the bead, R_b, and the penetration depth of the bead into the cell, δ_b, by

$$A_{mac} = 2\pi R_b \delta_b, \tag{1}$$

where

$$\delta_b = R_b - \sqrt{R_b^2 - R_{con}^2}. \tag{2}$$

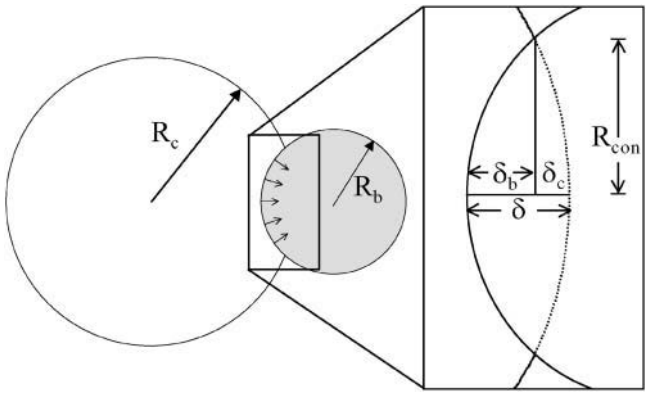

FIGURE 1 Schematic illustration of a neutrophil contacting a bead. The cell and bead radii are R_c and R_b, respectively. In the expanded view of the contact area, the total penetration depth, δ, is equal to the sum of the penetration of the bead into the cell, δ_b, and the cell into the bead, δ_c. The contact radius, R_{con}, is half of the contact length, which can be described as the chord between the cell and bead intersection perpendicular to the axis of penetration. The measured R_{con} was used to calculate the projected area, A_{proj}, and the macroscopic contact area, A_{mac}.

The quantity R_{con} is the contact radius of a circular cross section of the bead taken at the bead's penetration depth into the cell. We will refer to this cross-sectional area as the projected contact area, $A_{proj} = \pi R_{con}^2$. Substituting Eq. 2 into Eq. 1 results in the following expression to calculate the macroscopic contact area between a neutrophil and bead from measurements of R_b and R_{con}:

$$A_{mac} = 2\pi R_b \left(R_b - \sqrt{R_b^2 - R_{con}^2} \right). \tag{3}$$

Note that for all physically realizable cases, $0 \le R_{con} \le R_b$.

Force balance

An analysis based on static equilibrium was used to develop an expression to relate the contact radius (and A_{mac}) to the applied normal force, F, and the cortical tension of the neutrophil surface, T_{cort}. A force balance between the cell and the bead requires that the force equal the product of the pressure difference across the cell-bead boundary (ΔP_b) and the projected contact area, $F = \Delta P_b \times \pi R_{con}^2$. The pressure change across the cell and bead interface is

$$\Delta P_b = P_i + \frac{2T_{cort}}{R_b}, \tag{4}$$

where P_i is the pressure in the cell interior relative to the suspending fluid outside the pipette (Fig. 1) and T_{cort} is assumed to be constant and uniform over the cell surface. At static equilibrium, the internal pressure can be related to the cortical tension, $P_i = 2T_{cort}/R_c$, where R_c is the cell radius. (A slightly more accurate expression might be obtained by formally taking this force balance at the upstream side of the

cell. For a detailed discussion, see Appendix 1.) Using this expression, the relationships among the force, cortical tension, and dimensions of the system can be written as

$$F = 2T_{\text{cort}}\left(\frac{1}{R_b}+\frac{1}{R_c}\right)\pi R_{\text{con}}^2. \quad (5)$$

Solving Eq. 5 for R_{con}^2 and substituting the result into Eq. 3 results in the following expression for the macroscopic area of contact between the cell/bead surfaces at equilibrium:

$$A_{\text{mac}} = 2\pi R_b\left(R_b - \sqrt{R_b^2 - \frac{F R_c R_b}{2\pi T_{\text{cort}}(R_c+R_b)}}\right). \quad (6)$$

In the limit of infinite bead radius, this expression reduces to the simplified case describing the area of a liquid drop in contact with a flat surface, $\lim_{R_b\to\infty} A_{\text{mac}} = (F R_c)/(2T_{\text{cort}})$.

Dynamic analysis

We treat the neutrophil as a viscous drop with constant cortical tension and estimate the time-dependent changes in contact area when the neutrophil is pressed against a rigid bead. A small rigid bead impinging on a viscous spherical cell resembles the growth of a pendant liquid drop, the latter being a well-studied problem in fluid mechanics. In both situations, the introduction of a source of fluid at the sphere boundary (either by a bead displacing the inner cell volume, or by an inlet flow through a capillary nozzle) can cause essentially radial growth of the drop at sufficiently low flow rates. At higher flow rates from the nozzle into the drop, jetting occurs and there is considerable tangential convection within the drop. By balancing inertial, viscous, and interfacial forces in the growing drop, Humphrey et al. (1974) defined a dimensionless circulation number (C),

$$C = \frac{V^2\rho D_{\text{eq}}}{\gamma}\times\frac{V\rho D_{\text{eq}}}{\mu}, \quad (7)$$

as the product of modified Weber and Reynolds numbers. In the above definition, V is the maximum nozzle velocity, ρ and γ are the drop density and interfacial tension, and, for drops which are much more viscous than the surrounding phase, μ is the interior viscosity. D_{eq} is an equivalent diameter defined by

$$D_{\text{eq}} = \frac{R_{\text{con}}^2(R_{\text{con}}^2+4R_c^2)}{2R_c^3}, \quad (8)$$

where R_{con} replaces the nozzle radius and R_c is the drop radius. Through careful experimental visualization of the flow streamlines for a range of inner and outer fluids, Humphrey et al. (1974) showed that radial flow is predominant for values of C less than order unity. By analogy to the pendant drop problem, we may evaluate this dimensionless group to determine whether purely radial growth of the cell is to be expected during impingement, or whether a more complex interior flow with significant pressure gradients exists. Assuming characteristic values of $V = 1.0\ \mu$m/s, $\rho = 10^3$ kg/m^3 (1.0 g/cm^3), $D_n \approx 0.5\ \mu$m, $d = 8.0\ \mu$m, $\gamma = 2.5\times10^{-5}$ kg/s^2 (25 pN/μm), and $\mu = 100$ kg/m per s (100 pN s/μm^2 or 1000 poise), we obtain a circulation number of $C = O(10^{-22})$. (Note that 1.0 pN s/μm^2 = 1.0 N s/m^2 = 1.0 Pa s.) Thus, the interior flow induced by the impinging bead is predominantly radial, and we may proceed by modeling the cell deformation as the isotropic expansion of a viscous sphere.

The formulation of Scriven (1960) has been used to predict pressure and curvature changes of a drop growing on the tip of a capillary tube (MacLeod and Radke, 1993). To adapt this analysis to the indentation of the cell by a bead, we (conceptually) replace the flow from the capillary into the droplet with the volume displaced by the bead pushing into the cell. The governing equation describing the increase in the neutrophil (drop) radius, R_c, is (MacLeod and Radke, 1993)

$$P_i = \frac{2T_{\text{cort}}}{R_c} + \frac{4\kappa}{R_c^2}\frac{dR_c}{dt} + \frac{4\,\Delta\mu}{R_c}\frac{dR_c}{dt}, \quad (9)$$

where P_i is the pressure in the cell interior relative to the ambient pressure in the measurement chamber, κ is the interfacial dilatational viscosity, $\Delta\mu$ is the viscosity difference across the neutrophil surface, and dR_c/dt is the radial velocity of the cell boundary. The pressure driving the inflation of the cell (analogous to the capillary pressure in the growing drop model) comes from the pressure difference across the cell surface at the cell-bead interface,

$$P_i = \frac{F}{\pi R_{\text{con}}^2} - \frac{2T_{\text{cort}}}{R_b}. \quad (10)$$

(In Appendix 2 we consider the possibility that local viscous resistance in the cytoplasm near the bead impingement might affect this expression for the pressure.) The second term in Eq. 10 (containing the cortical tension) is constant, whereas the first term changes as both the contact radius R_{con} and the force F increase with time. The increase in R_{con}^2 lags the increase in force, such that the first term exceeds the second, driving the increase in R_c as the bead indents the cell. As R_{con} continues to increase, the first term will eventually approach the second as the equilibrium condition described in Eqs. 4 and 5 is reached. Combining Eqs. 9 and 10 yields the following expression to model neutrophil deformation as a function of time,

$$\frac{dR_c}{dt} = \left[\frac{FR_c}{4\pi R_{\text{con}}^2} - \frac{T_{\text{cort}}R_c}{2}\left(\frac{1}{R_b}+\frac{1}{R_c}\right)\right]\left(\frac{\kappa}{R_c}+\mu\right)^{-1}, \quad (11)$$

where $\Delta\mu$ has been replaced with μ because the external viscosity is much smaller than the cytoplasmic viscosity.

In Eq. 11, F, R_c, and R_{con} are all functions of time. The force depends on the difference between the instantaneous cell velocity and the free stream velocity. Thus, F increases as the cell decelerates during impingement. The relationship between force and velocity has been derived by Shao and Hochmuth (1996) as

$$F = \pi R_p^2 P_{im}(1 - U_i/U_f)/C_1, \tag{12}$$

where R_p is the pipette radius, P_{im} is the measured impingement pressure, U_i is the instantaneous velocity of the cell in the tube, and U_f is the free velocity of the cell in the tube at the same pressure. The constant term C_1 is

$$C_1 = 1 + \frac{4\varepsilon}{3} + \frac{16(L_{eq} - D_c)}{9\pi R_p}\left(\varepsilon^{5/2}\sqrt{2} - \frac{4\varepsilon^3}{\pi}\right), \tag{13}$$

where D_c is the diameter of the cell, L_{eq} is the equivalent tube length of the pipette, and $\varepsilon = (R_p–R_c)/R_c$ is the dimensionless film thickness between the cell and the wall of the pipette. The equivalent tube length is determined from the free velocity U_f of the cell in the tube for a given pressure (Shao and Hochmuth, 1996),

$$L_{eq} = \left[\frac{R_p P_{im}}{\mu_s U_f} - 4\pi\left(\frac{2}{\varepsilon}\right)^{1/2} + \frac{71}{5}\right]\frac{3R_p}{24 - 32\varepsilon}, \tag{14}$$

where μ_s is the viscosity of the suspending solution in the pipette (0.97 cP at 22°C). Note that when $U_i = U_f$, the force given in Eq. 12 is zero. As the cell impacts the bead, its instantaneous velocity decreases as the depth of penetration of the bead into the cell (δ) increases. Thus, as the bead pushes into the cell, the cell velocity is simply $U_i = d\delta/dt$.

Solution of Eq. 11 requires additional relationships between the penetration depth δ, the contact radius R_{con}, and the instantaneous cell radius R_c. From simple geometry, R_{con} is related to δ and R_c as

$$R_{con}^2 = 2R_b\delta\left(\frac{R_c - \delta/2}{R_c + R_b - \delta}\right) - \delta^2\left(\frac{R_c - \delta/2}{R_c + R_b - \delta}\right)^2. \tag{15}$$

To obtain δ as a function of R_c, we apply the condition that the cell volume remains constant. This leads to the following fourth-order expression (Kern and Bland, 1948),

$$\begin{aligned} 0 = &-\delta^4 + 4\delta^3(R_c + R_b) - 12\delta^2 R_c R_b + 16\delta(R_o^3 - R_c^3) \\ &+ 16(R_c^4 + R_c^3 R_b - R_c R_o^3 - R_b R_o^3). \end{aligned} \tag{16}$$

Taking the derivative of Eq. 16 with respect to time, we can relate the rate of change of δ to the rate of change of R_c,

$$\frac{d\delta}{dt} = \frac{dR_c}{dt} \times G(t), \tag{17}$$

where

$$G(t) = \frac{\delta^3 - 3\delta^2 R_b - 12\delta R_c^2 + 16R_c^3 + 12R_c^2 R_b - 4R_o^3}{\delta^3 - 3\delta^2(R_c + R_b) + 6\delta R_c R_b - 4(R_o^3 - R_c^3)}. \tag{18}$$

Combining Eqs. 11, 12, and 17, we obtain the governing equation for the cell-bead impingement driven by pressure in a pipette,

$$\frac{dR_c}{dt} = \frac{P_{im}R_p^2 - 2R_{con}^2 C_1 T_{cort}(1/R_b + 1/R_c)}{4\mu R_{con}^2 C_1/R_c + P_{im}R_p^2 G(t)/U_f}. \tag{19}$$

It is also of interest to calculate the contact stress between the two surfaces as a function of time because it is the stress that should correlate with alteration of surface microtopography. The contact stress, $\sigma = F/\pi R_{con}^2$, is calculated by recognizing the appearance of this term in Eq. 11. Once the dependence of R_c on time is known for a given cell and impingement pressure, σ can be calculated directly according to

$$\sigma = \frac{4}{R_c}\left(\frac{\kappa}{R_c} + \mu\right)\frac{dR_c}{dt} + 2T_{cort}\left(\frac{1}{R_b} + \frac{1}{R_c}\right). \tag{20}$$

Note that at equilibrium, the first term is zero, and the contact stress is given by the second term, which is independent of force. An implicit assumption here is that the cortical tension remains constant with area expansion, an assumption that is supported by a previous study (Needham and Hochmuth, 1992).

Predictions of the temporal evolution of the contact area for experimentally relevant conditions were obtained using MATLAB (Rel. 12, The MathWorks, Natick, MA). Eq. 19 was integrated numerically to determine R_c as a function of time. For a given value of R_c, δ was obtained by choosing the root of Eq. 16 satisfying $0 \le \delta < R_b$. (Only one root satisfied this condition.) This value of δ was used to calculate R_{con} via Eq. 15. The contact radius was then used in Eq. 3 to calculate the area of contact between the two surfaces at each time step.

Shear rate

The apparent viscosity of the neutrophil has been shown to depend on the shear rate (Tsai et al., 1993; Drury and Dembo, 2001). As a basis for choosing appropriate values for the cell viscosity in the analysis, the shear rate within the cell during indentation was estimated by forming the ratio of a characteristic velocity (V_c) divided by a characteristic length scale over which the velocity is expected to vary by an amount $\sim V_c$. In our problem, the only characteristic velocity scale is the velocity of the cell during impingement with

the bead. The characteristic length is obtained from the analogous problem of pendant-drop growth as described above. D_{eq} was first suggested by Humphrey et al. (1974) as the equivalent diameter that preserves the relative importance of nozzle diameter to drop volume (Eq. 8). By analogy we take the nozzle diameter to be equal to the time-averaged contact radius. This gives a value of D_{eq} in the range 0.9–1.8 μm. For each impingement, we take the characteristic shear rate as the ratio of

$$\dot{\gamma} = \frac{\langle d\delta/dt \rangle_c}{D_{eq}(\langle R_{con} \rangle)}, \tag{21}$$

where the angled brackets indicate the time-averaged value over the first 1.0 s of contact,

$$\langle x \rangle = \int_0^1 x(t)dt. \tag{22}$$

To match the analytical prediction to measured values, a least-squares regression was performed first with the viscosity set to zero. From this fit, the characteristic shear rate was calculated, and the cell viscosity was obtained from the power law fluid description given by Tsai et al. (1993),

$$\mu = 130 \times \left(\frac{\dot{\gamma}}{\dot{\gamma}_o}\right)^{-0.5}, \tag{23}$$

where $\dot{\gamma}_0 = 1.0\,s^{-1}$ and the viscosity is expressed in units of pN s/μm^2 (1.0 pN s/μm^2 = 1.0 Pa s = 1.0 kg/m per s = 10 poise).

MEASUREMENT METHODS

Cell preparation

The cell preparation and system setup for the touch experiments has been adapted from a similar setup previously described (Spillmann et al., 2002) and based on the original methods of Shao and Hochmuth (1996). Neutrophils were obtained from a drop of whole blood via a finger stick and diluted into Hank's Balanced Salt Solution (without Ca^{2+} or Mg^{2+}), 10 mM HEPES, and 4% heat-inactivated fetal bovine serum (FBS, Hyclone, Logan, UT), pH 7.4, 290 mOsm. The suspending solution for measuring cell deformation contained 10 mM HEPES, 5 mM $MgCl_2$, 145 mM NaCl, 5 mM KCl, 2 mg/ml glucose, 0.5 mM EGTA, and 4% FBS, pH 7.4, 290 mOsm. Micropipettes were filled with the suspending solution, minus FBS.

Micropipette preparation

Micropipettes were made from glass capillary tubing (Freidrich and Dimmoch, Millville, NJ) heated and pulled in a vertical pipette puller (Model 730; David Kopf Instruments, Tujunga, CA). Two successive pulls produced the desired taper and an extended, thin tip of the proper diameter. Pipettes were formed by breaking off the tips in a microforge consisting of a micromanipulator and a heated lead-glass bead mounted on a microscope stage. Pipettes used to hold the bead were ~2 μm in diameter, and pipettes used for cell transfer and translation of neutrophils for touch experiments were 9–10 μm in diameter. Pipettes were coated with Surfasil (Pierce, Rockford, IL) according to the manufacturer's protocol and stored at room temperature overnight in a closed environment.

Touch experiments

Diluted blood was placed in a chamber formed by a Plexiglas spacer between two Surfasil-coated coverslips. Both this chamber and an adjacent one, the touch chamber, were placed on the stage of an inverted light microscope (Diaphot, Nikon, Garden City, NY) and partly enclosed with an apparatus providing humidified air to minimize evaporation. Experiments were performed in the touch chamber, which was filled with the suspending buffer plus a dilute suspension of either M-450 or M280 Dynabeads (Dynal, Lake Success, NY). The chamber had openings on opposite sides to accommodate opposing micropipettes. The holding pipette and the translation pipette were filled with buffer and positioned inside the touch chamber. A slight negative pressure was then applied to both pipettes for ~15 min to draw protein solution into the pipette tip to reduce unwanted neutrophil adhesion to the glass. Using the translation micropipette, neutrophils were chosen and transferred into the touch chamber and allowed to equilibrate for at least 20 min with the suspending solution. All measurements were performed at room temperature (22°C).

After cell transfer, the two micropipettes, mounted on micromanipulators, were aligned opposite one another in the touch chamber. A bead was captured and held in the holding pipette by a negative aspiration pressure, and a neutrophil was aspirated into the translation pipette, which had a diameter large enough to allow the neutrophil to translate freely through its lumen, as shown in Fig. 2 *A*. The zero pressure inside the translation pipette was determined by raising or lowering reservoir 1 until the neutrophil was stationary inside the pipette. To start a touch sequence a positive pressure (P_{im}) was imposed on the cell by displacing the reservoir connected to the translation pipette upward relative to the zero point. A digital micrometer provided a measure of the impingement pressure, which ranged from ~1.0 to ~6.0 pN/μm^2 (0.1–0.6 mm H_2O). A withdrawal pressure of 2.0–5.0 pN/μm^2 was established by adjusting airflow using a valve to regulate the suction rate generated by a vacuum pump and monitored using a transducer. The positive pressure was used to drive the neutrophil into contact with the bead in the holding pipette for a user-defined time of ~2 s, at which time a solenoid valve (Lee Company, Westbrook, CT) was engaged to introduce the withdrawal pressure. When the neutrophil had moved away from the contact zone, another impingement could begin. Time between contacts was three or more seconds. The holding pipette was kept approximately one neutrophil diameter inside the translation pipette throughout the experiment to maintain alignment of the neutrophil with the bead (Fig. 2 *B*). Additionally, minor adjustments to the translation pipette were made throughout an experiment to maintain the best axial alignment between the two surfaces. If significant asymmetries in the cell motion during contact were observed, data were discarded and the cell and bead realigned by matching the focus of the bead and the pipette.

Each touch sequence was recorded on videotape with a time stamp and the withdrawal and impingement pressure overlaid on the image. Zero pressure in the translation pipette was checked periodically for drift in the pressure due to evaporation of fluid from the meniscus of the touch chamber. Typically such corrections were <0.5 pN/μm^2 (0.05 mm H_2O). The contact area was determined by measuring the contact length ($L_{con} = 2R_{con}$) from video recordings. Distances were calibrated using a stage micrometer.

Methods for obtaining self-consistent parameter values

Procedures were implemented to check for and minimize possible errors in our force calculations. We took advantage of the expectation that the free stream velocity of the cell before contact should be proportional to the impingement pressure. In most cases the expected linear relationship was observed (Fig. 3 *A*). For the cases in which linearity was not observed, a progressive change in the cell velocity with time indicated some drift in the applied pressure. For these cases, data obtained immediately after calibration of the zero pressure proved to be consistent with the linear expectation, and only these data were used in the calculations (Fig. 3 *B*). In addition, we used the knowledge that the equivalent pipette length (L_{eq}) should be the same for all cells measured using the same pipette to make sure that self-consistent

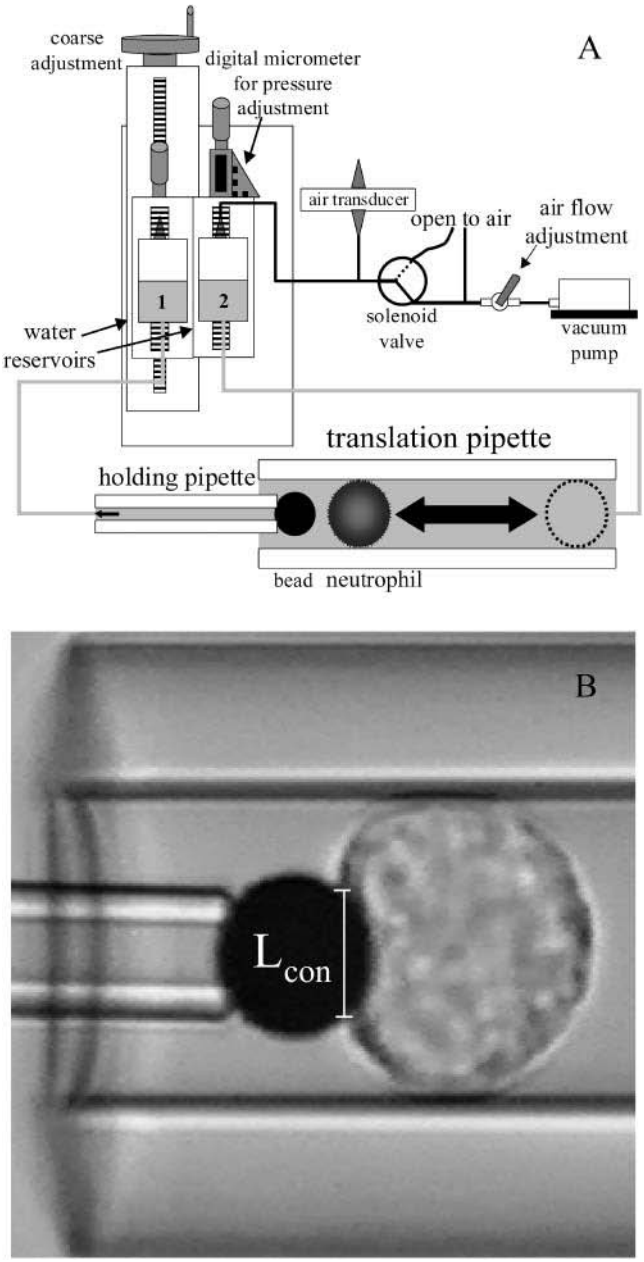

FIGURE 2 System for controlling neutrophil/bead contact. (*A*) The two pipettes were positioned in a chamber on the stage of a light microscope and connected to adjustable water reservoirs. A positive pressure on the neutrophil was produced by raising reservoir #2 by a measured distance relative to the position at which flow in the pipette stopped. A vacuum pump connected to reservoir #2 via a solenoid valve provided the withdrawal pressure to draw the neutrophil away from the bead. To withdraw the cell from its contact with the bead, suction was applied by activating the valve via a computer interface. To initiate the next contact, the valve was turned off, and the positive pressure set by the reservoir height pushed the cell into contact with the bead. (*B*) Video micrographs showing the contact between a neutrophil and 4.5-μm diameter bead. Images were taken near the end of a 2-s contact, showing the cell bead pair at equilibrium. In this example, the impingement pressure was 4.4 pN/μm^2, and the contact force was 235 pN.

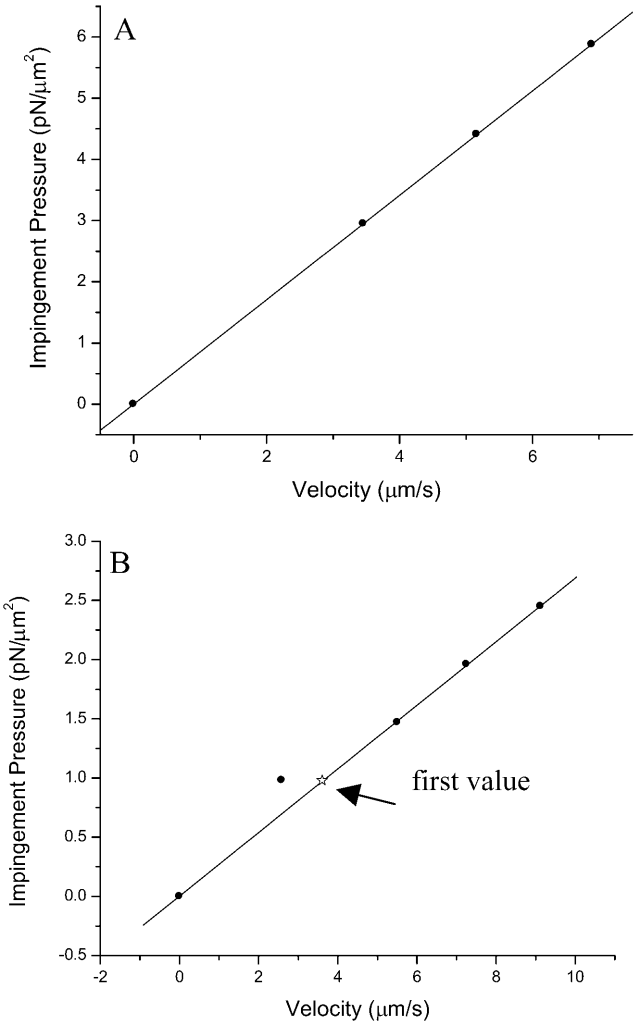

FIGURE 3 Self-consistency tests for the pressure values. The impingement pressure is plotted versus the free velocity of the cell in the pipette before contacting the bead. The expected linear relationship was obtained in most cases (*A*). In *B* an example is shown in which the expected linearity was not observed. The star shows that the first point measured at that pressure after setting the zero point is consistent with the expected linear relationship. The linear slopes give the value of P_{im}/U_f which is used to determine the value of L_{eq} (Eq. 14) that is used to calculate the force (Eqs. 12 and 13).

values for the gap width parameter ε were used for all cells measured with the same pipette. First, values for ε were estimated from measurements of the cell and pipette diameters. Then L_{eq} was calculated for each cell from measurements of the dependence of the free velocity on impingement force (Eq. 14). The average L_{eq} for all cells tested with a given pipette was then taken as the ''true'' value, and then the gap parameter ε was recalculated for each cell via Eq. 14 using the true L_{eq} and the measured ratio of P_{im}/U_f. Although this approach does not eliminate systematic errors of measurement, self-consistent values were obtained.

RESULTS AND COMPARISON TO THEORY

Static equilibrium

Repeated tests were performed on 19 cells from four donors. Each cell was tested at each of four impingement pressures.

Contact duration was ~2 s for each touch. In calculating the force, corrections were made for fluid leak around the cell according to Eqs. 12 and 14. The measured free stream velocity for a given pressure varied depending on the shape of the pipette tip and the size of the gap between the cell and the pipette wall. For the cells and pipettes used in the present study, the parameter ε ranged from ~0.02 to 0.12. For pressures of 2.5–3.0 pN/μm^2, free stream velocities ranged from 2.5 μm/s to 12 μm/s, giving equivalent tube lengths ranging from 600 to 4000 μm. When these values are applied via Eq. 13 the contributions to the force of the terms containing ε ranged from 0.07 to 1.27, although for over 85% of the cells tested the corrections were between 0.2 and 0.8. Thus, the ε-containing terms in Eq. 13 had a significant effect on our calculations of force, and could not be neglected.

Measurements of the contact radius R_{con} as a function of force were used to estimate the cortical tension of the cells (Eq. 5). In making these calculations we recognize the potential for systematic overestimation of the contact zone due to misalignment of the cell and the bead or errors in measurement due to the overlap of diffraction patterns as the cell and the bead come into contact. These errors were largest when the contact area was small, either when small beads or low forces were used. Therefore, in determining the cortical tension, we used the mean projected areas for each of the 12 cases where large beads were used and confined the data set to the highest impingement pressures applied. A weighted linear regression to Eq. 5 (mean values were weighted by the inverse of the variance of 25 repeated measurements) yielded a value for the cortical tension of 21.7 pN/μm for T_{cort}. If the regression was fixed at the origin, a tension of 23.2 pN/μm was obtained (Fig. 4 *A*). These values were consistent with the behavior for data obtained at all impingement pressures, as can be seen by comparing the measurements with the prediction for contact area as a function of force given in Eq. 6. As illustrated in Fig. 4 *B*, the data show good agreement with the predictions for cortical tensions ranging from 16 to 24 pN/μm. This is at the low end of the range of published values (Table 1).

Dynamic response

The contact area was measured as a function of time for cells contacting the beads under constant force. Cells and beads were contacted 25 times, and the 1st, 6th, 11th, 16th, and 21st touches were measured and averaged, except when there was evidence for drift in the pressure, in which case the first sequence after zero pressure calibration was used. To correlate the measurements with the theoretical predictions, the cortical tension was set equal to 20 pN/μm and two successive nonlinear regressions to the data were performed. In the first, three free parameters were determined: a constant offset for time, a constant offset for the contact radius, and viscosity. The results of this first regression were used to obtain the characteristic shear rate. Then the shear rate was

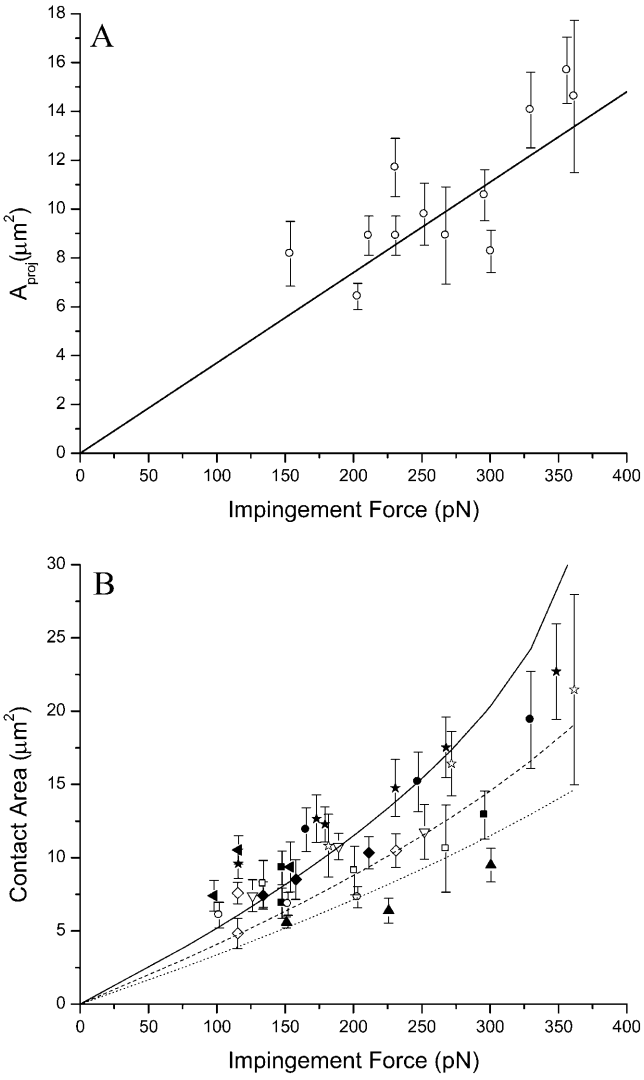

FIGURE 4 (*A*) The equilibrium projected area of contact (πR_{con}^2) as a function of the applied force. The average equilibrium projected area at the largest impingement force is shown for each of 12 cells contacting 4.5-μm diameter beads. Error bars represent the standard deviation for 25 repeated measurements. In performing the linear regression each point was weighted as 1/variance of the 25 measured values. The slope of the linear regression was used to calculate the cortical tension according to Eq. 5. When the regression was fixed at the origin, the calculated value for T_{cort} was 23.2 ± 0.7 pN/μm. If the intercept was not fixed at zero, the regression yielded an intercept of −0.65 μm, and T_{cort} was calculated to be 21.7 ± 4.6 pN/μm. (The ±values indicate the standard error of the fitted parameters.) (*B*) Relationship between the contact area and impingement force of neutrophil/bead in static equilibrium. Each different symbol represents a different cell and error bars correspond to standard deviations for ~25 repeated measurements at each pressure. Overlaid across the measurements are model predictions of the contact area as a function of force (Eq. 6). (The three curves correspond to predictions for different cortical tensions: *solid curve*, 16 pN/μm; *dashed curve*, 20 pN/μm; and *dotted curve*, 24 pN/μm.) Average values for the cell and bead radii used to fit the data were 4.4 μm and 2.4 μm, respectively.

TABLE 1 Comparison of the calculated neutrophil cortical tension, T_{cort}

T_{cort} (pN/μm)	Source
16–24	Current study
13	Evans and Kukan (1984)
35	Evans and Yeung (1989)
24	Needham and Hochmuth (1992)
27	Tsai et al. (1993)

used in Eq. 23 to obtain the cell viscosity, and a second fit was performed with the viscosity set to this value. The characteristic shear rate for the second fit differed from the one for the first fit by $<4\%$, a reflection of the relative insensitivity of the fit to the value of the viscosity. In Fig. 5 are shown example fits to the average of five time-courses measured at each of three different impingement pressures for large and four different pressures for small beads. Values for the fitted offsets for all data were 0.003–0.038 s for the time, and 0.27–0.51 μm for the contact radius. Also shown are the calculated indentation depths, δ, as a function of time (Fig. 5, *C* and *D*).

Contact stress

Examples of the calculated time-course of the contact stress are shown in Fig. 6 for seven different impingement pressures. The data on which the curves are based are the same as that shown in Fig. 5. Note that the same equilibrium contact stress is approached for beads of the same diameter, but that the equilibrium stress is higher for small beads (36 pN/μm^2) compared to large beads (26 pN/μm^2). Also note that there is a transient increase in stress that is up to twice the equilibrium value for the largest pressures applied. To evaluate the effect of contact stress on adhesion in cell-bead contact experiments, it is instructive to examine how the mean contact stress (averaged over the contact duration), $\langle\sigma\rangle$, changes with impingement force and contact time (see Fig. 6 *B*). For contact times <0.5 s, the difference between the time-averaged stress and the equilibrium stress can be significant, approaching a factor of 2 in the worst case tested. But for two-second contacts there is little difference between the time-averaged contact stress and the equilibrium value ($<20\%$).

DISCUSSION

Cell deformation during leukocyte recruitment

The present study is motivated by a desire to understand the role that mechanical forces play in the complex interactions between neutrophils and the vascular endothelium during neutrophil recruitment. Clearly, the chemistry of receptor-ligand interactions and intracellular signaling events that affect bond chemistry are critical for effective recruitment of leukocytes from the circulation, but deformation also makes a significant contribution to recruitment. An early study in vivo by Firrell and Lipowsky (1989) indicated that cell deformation alters the balance between adhesive and hydrodynamic shearing forces by increasing the area of contact and prolonging the contact duration in the presence of shearing forces. This behavior has been further studied and modeled by several investigators (Dembo et al., 1988; Alon et al., 1995; Dong et al., 1999; Lei et al., 1999; Dong and Lei, 2000). Most of these analyses treat the cell with a two-dimensional approximation of an elastic ring surrounding a viscous core, and examine the effects of mechanical forces on the peeling rate at the trailing edge of a cell subjected to fluid shear forces. All show significant effects of cell deformation on the dynamics of the cell-substrate interaction, although none consider possible effects of force on the *formation* of adhesive bonds.

One of the criticisms raised concerning existing analyses of cell-substrate interactions in fluid shear is that the approximate, two-dimensional descriptions of the cell (or the failure to treat cell rheology at all) limits the reliability of quantitative predictions obtained using these approaches. The complex rheological behavior of the actual cell and the coupling of cell deformation to the kinetics of bond formation and breakage in the contact zone, make it extremely difficult to develop realistic three-dimensional treatments of an adherent cell subjected to fluid shear. To avoid this complexity, but to gain a better understanding of how mechanical forces might affect bond formation, we have chosen an experimental system more amenable to realistic mechanical analysis. The axisymmetry of the deformation and loading in our experiments and the ability to regulate and calculate forces between the cell and the bead make it possible to make accurate predictions of the size of the contact zone and the contact stress between the cell and the substrate (Shao and Hochmuth, 1996; Ritchie and Evans, 1997; Chesla et al., 1998; Tees et al., 2001).

Constitutive models of the cell

The need for leukocytes to deform as they circulate through the microvasculature has motivated extensive efforts to model and characterize their rheological properties (Yeung and Evans, 1989; Needham and Hochmuth, 1990; Tsai et al., 1993; Drury and Dembo, 2001). An early report based on small deformations of neutrophils into a micropipette used the model of a standard viscoelastic solid to model cell behavior for small deformations (Schmid-Schonbein et al., 1981). Subsequently, observations of large cellular deformations demonstrated that neutrophil behavior is fundamentally fluid-like: cells deform continuously into micropipettes in response to constant loads. These observations led to the model of the cell as a viscous fluid with a constant cortical tension, a liquid-drop model (Evans and Kukan, 1984; Evans and Yeung, 1989; Needham and Hochmuth, 1990). In the simplest case, the neutrophil cytoplasm is modeled as

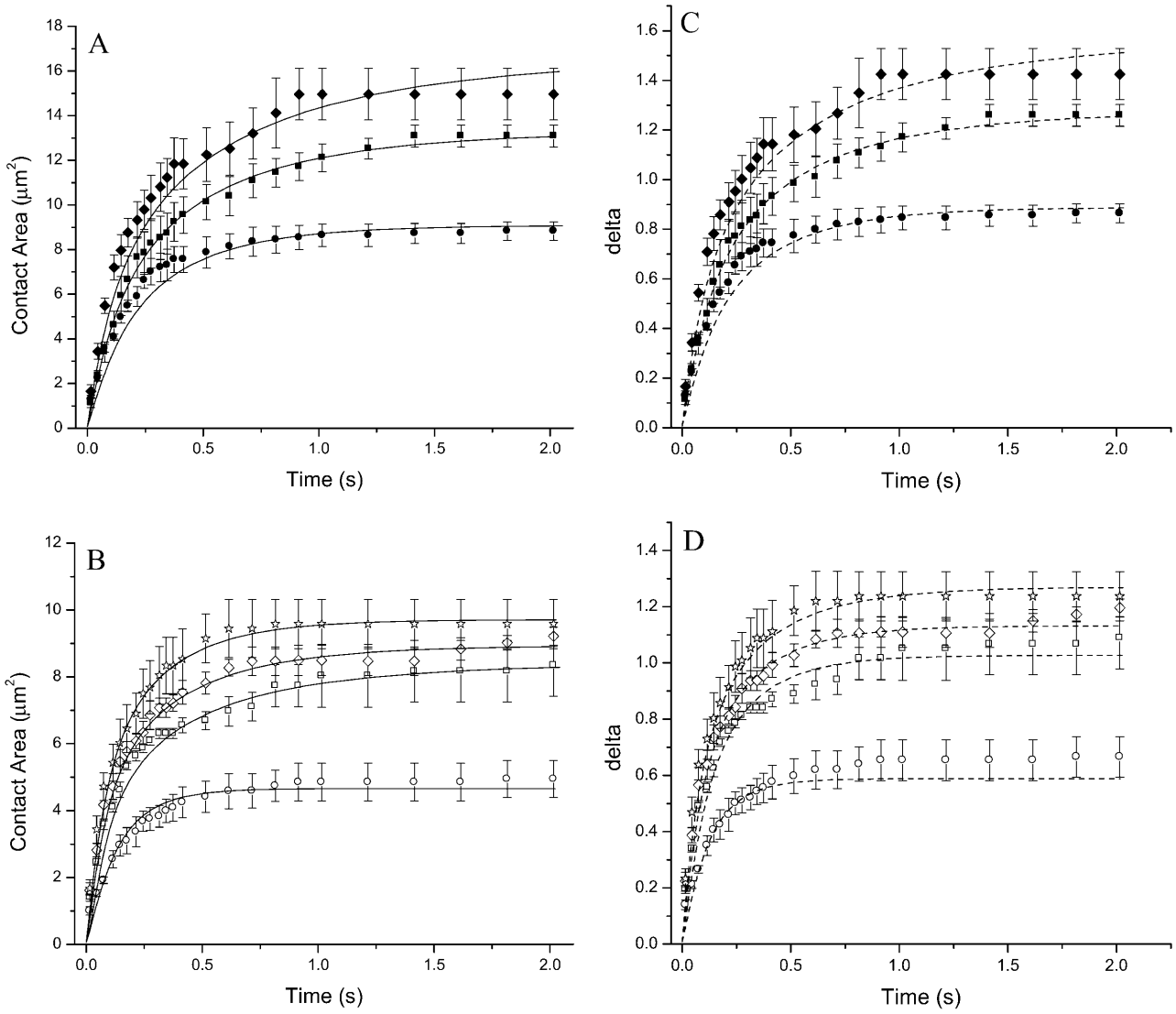

FIGURE 5 Time dependence of the contact area during cell-bead contact under a constant impingement pressure. A representative neutrophil is shown. Error bars show the standard deviation at each time point for five replicate measurements (from five different contact events). (*A*) Impingement with 4.5-μm beads. Equilibrium forces were 115 pN (●), 170 pN (■), and 230 pN (♦). Solid curves are the model predictions based on Eq. 19 and using a cellular viscosity consistent with the characteristic shear rate (Eq. 21). (*B*) Similar results were obtained when small (2.8-μm diameter) beads were used. Equilibrium forces were 50 pN (○), 80 pN (□), 100 pN (◇), and 130 pN (☆). In *C* and *D* the corresponding values of the indentation depth δ are shown. Note that the dashed curves were obtained from the fitted curves in *A* and *B*, and are not direct regressions to the values of δ.

a simple Newtonian fluid, but a number of embellishments to the simple fluid-drop model have been proposed. Motivated by ultrastructural evidence of a dense cortical layer of actin in these cells, a model was proposed in which there is a distinct viscous resistance from the cortical region of the cell (Evans and Yeung, 1989; Yeung and Evans, 1989). In a subsequent study, observations of differences in the apparent viscosity of the cell measured at different rates of deformation revealed that the cytoplasm exhibits shear thinning behavior (Tsai et al., 1993). Shear thinning behavior was also included in a model presented by Drury and Dembo (2001), who combined shear thinning and a surface viscosity component to account for experimental results from micropipette aspiration experiments performed over a wide range of conditions. Recently, Herant et al. (2003) examined a more comprehensive model to account for neutrophil behavior in both passive and motile states. They also concluded that the cortical region of the cell plays a predominant role in its viscous (dynamic) response (Herant et al., 2003), but only when the surface deformations exceed 5%, a condition not generally met in the indentation studies described in the present report.

In the present analysis we have elected to treat the cell as a fluid drop with a uniform viscosity and constant cortical tension. This choice is somewhat arbitrary because, for the

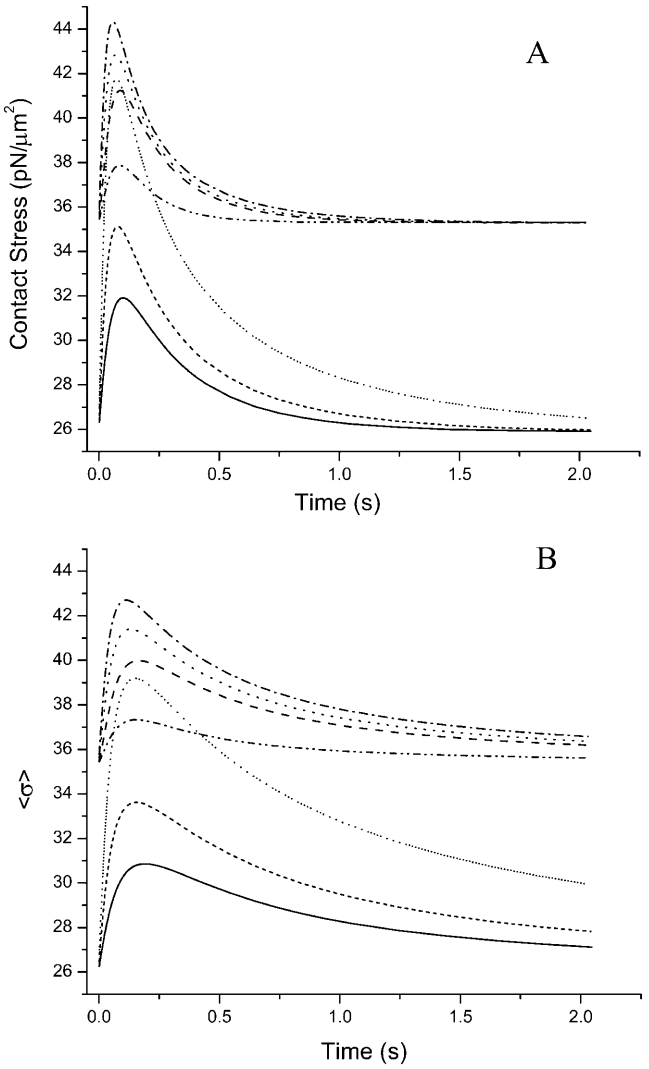

FIGURE 6 (*A*) The time dependence of the contact stress over a 2-s contact time. The contact stress was calculated via Eq. 20 based on the fitted curves to the data in Fig. 5. The stress for contacts with small (2.8-μm diameter) beads (*upper curves*) approach an equilibrium stress of 36 pN/μm, and for large (4.5-μm diameter) beads (*lower curves*), 26 pN/μm. Impingement pressures for the small beads were ~1.0, 1.5, 2.0, and 2.5 pN/μm^2, and for the large beads, 3.0, 4.5, and 6.0 pN/μm^2. In each group the size of the transient increase in contact stress increased with increasing force. (*B*) The contact stress shown in *A* was integrated over time, and the time-averaged value is shown as a function of increasing contact duration. For contacts <0.5 s, there can be substantial differences between the time-averaged stress and the equilibrium stress. For longer times, the time-averaged value approaches the equilibrium value, such that for 2-s contacts, the time-averaged stress is within 20% of the equilibrium value for large beads, and within 5% for the smaller beads.

small deformations produced in the present experiments, a variety of mechanical models can match the data, particularly when material coefficients are chosen freely. To some extent our choice is justified by the fact that the cellular behavior we observe is entirely consistent with published values for the material coefficients. Specifically, values of the cortical tension obtained in the present study agree closely with previously published values (Table 1). This agreement exists despite possible errors in our measurements. The most significant errors are likely to come from two sources. Errors in our estimation of the gap width between the cell and the wall of the pipette may lead to errors in the calculated force on the cell, and misalignment of the cell and bead during contact may lead to systematic errors in our estimate of the contact area. As described in Results and Comparison to Theory, above, the contributions to the force of terms in Eq. 13 containing the gap width ranged from 0.07 to 1.27. Our approach of calculating these terms using measurements of the free cell velocity in the pipette to obtain self-consistent values for different cells tested using the same pipette was designed to minimize both the magnitude of random errors and variability in the accuracy of the force calculated for different cells. An additional error could result from changes in the cell diameter when it contacts the bead. To estimate the magnitude of this error, careful measurements of the change in cell dimensions were made immediately before contact and at the equilibrium contact for the cases in which these terms contributed most significantly to the calculated force. (Although there may be uncertainties in the absolute values of the cell and pipette diameters, accurate measurements of changes in the gap size between the cell and pipette can be made by choosing consistent locations in the diffraction patterns of the image.) Using this approach we estimate that cell deformation during contact may have resulted in an underestimation of the force by ~25% for the worst case. Errors in the calculated contact area due to misalignment of the cell and bead were also a concern. Whenever a significant deviation from axial alignment was observed, the data were discarded, and the cell and bead realigned for subsequent contacts. Concerns over significant systematic errors in our measurements are alleviated by our observation that the equilibrium contact area measurements as a function of force extrapolate to a value close to zero (Fig. 4).

Interestingly, we find that agreement between analytical prediction and experiment for the dynamic response is relatively insensitive both to the value of the cell viscosity and to whether the viscous dissipation occurs primarily in the cortex or throughout the cell interior. The inability to distinguish between cortical and bulk viscosity is evident from Eq. 9, where it can be seen that the cortical viscosity κ enters the analysis in the same manner as the bulk viscosity μ, except for division by R_c, which changes little during the indentation process. Thus μ and κ/R_c behave as equivalent constants in the analysis. The insensitivity of the analytical prediction to the value of the viscosity can be understood by examining the two terms in the denominator of Eq. 19. The second term evaluates to ~2000 pN/s per μm. In the first term, the terms multiplying the viscosity evaluate to a value on the order of 1.0 μm. The cellular viscosity is on the order of 200 pN/s per μm^2, making the first term an order-of-magnitude smaller than the second. Thus, small changes in the viscosity term

(note that this includes both cortical and cytoplasmic viscosity) affect the predictions very little because the second term in the denominator of Eq. 19 dominates the behavior of the system.

Contact stress and the importance of microtopography

The microtopography of the cell surface also plays a significant role in determining the ability of neutrophils to form specific bonds with substrate. Direct evidence for this comes from a study showing that differences in surface topology can result in a 50-fold change in the effective binding affinity of receptors confined to surfaces (Williams et al., 2001). This effect is thought to arise from several mechanisms. A simple physical effect of surface roughness is that only portions of the cell surface come into intimate contact with a smooth substrate, limiting the actual contact area where molecular bonds can form. In addition, an uneven distribution of adhesion receptors over the neutrophil surface and the lateral mobility of receptors on the membrane will affect bond formation in ways that are intrinsically connected to surface microtopography. It is significant that L-selectin molecules, which are important in the initial formation of bonds during neutrophil recruitment, are localized to the tips of the microvilli (Erlandsen et al., 1993; Bruehl et al., 1996). In contrast, other receptors such as the β_2-integrin Mac-1, which appear to function primarily after initial capture during cell arrest and migration, are localized away from the microvilli tips (Erlandsen et al., 1993). Thus, changes in surface microtopography brought about by active cytoskeletal reorganization or by passive deformation of the cell surface under contact loads are likely to have substantial effects on the formation of adhesive bonds.

The present study provides a basis for understanding the role of force in modifying neutrophil topography. The degree of alteration of the microtopography by deformation of microvilli should depend on the force per microvillus in the contact zone. Therefore, the critical parameter for predicting alteration of surface topography in response to force is not the total force, but the force per unit area (contact stress). We have seen that the macroscopic contact area at equilibrium depends on the magnitude of the impingement force (Eq. 6), but that the increase in area with force is such that the contact stress is independent of force (Eq. 20). As the contact area increases under compression, the number of microvilli within this area increases proportionately. Thus, for equilibrium contacts at different forces, one would not expect to observe differences in behavior due to effects of altered microtopography. For the experimental approach considered here, this prediction should also hold for dynamic situations in which the contact stress transiently increases above the equilibrium value. Even though there are significant elevations of stress during the first 0.5 s of contact, the time-averaged contact stress remains close to the equilibrium value, deviating by $<20\%$ for a contact duration of 2.0 s.

The effect of force on microtopography would naturally depend on how the microvilli respond to compression forces. For a typical cell ($\sim$9 μm diameter) contacting a bead with a diameter of 5 μm, and a cortical tension of 20 pN/μm, the contact stress relaxes to an equilibrium value of $\sim$26 pN/μm^2. A previous report by Shao et al. (1998) studied the effect of mechanical forces on microvilli in extension and found that they behave as springs with a spring constant of $\sim$40 pN/μm. (We are unaware of any studies that have examined microvilli in compression.) Based on an estimate of $\sim$5 microvilli/μm^2 (Shao et al., 1998), a contact stress of 26 pN/μm^2, the estimated force per microvillus would be $\sim$5 pN/microvillus, sufficient to cause a small but appreciable deformation of the surface. (Using the spring constant for extension, a reduction in microvillus length of 125 nm is predicted. This is a substantial percentage of the typical microvillus height of 100–300 nm.) For a smaller bead, the equilibrium stress would be higher ($\sim$36 pN/μm^2), and the expected surface deformation would be greater. These calculations indicate that the effect of contact stress on adhesion probability could be substantial.

CONCLUSIONS

The mechanical behavior of neutrophils impinging a rigid substrate is found to be consistent with analytical predictions based on a model of the cell as a liquid drop and using published values for the cellular properties. At equilibrium, the measured contact area as a function of force yields values of the cortical tension that are in close agreement with published values. The dynamic response of the cell during the impingement process was also found to be consistent with predictions based on the behavior of a fluid drop, although, for the experimental system examined here, the predicted behavior was relatively insensitive to the value chosen for the viscosity. Although it is likely that other models might also be used to make accurate predictions of this behavior, the liquid-drop model has shown excellent fidelity with observed cellular behavior over a wide range of conditions. Two important conclusions are reached that are relevant to the role of mechanical force in modifying the contacts between a neutrophil and a rigid substrate. First, under axial loading, the contact stress is independent of the magnitude of the applied force because the increase in contact area simply distributes the total force over a larger area. The contact stress is, however, predicted to depend on the curvature of the substrate. Second, even accounting for changes in the contact stress during the loading process for the experimental system considered, the maximum deviation from equilibrium is less than a factor of 2, and the time-averaged stress for contacts of 2 s or more is within 20% of the equilibrium value. These conclusions are used in a companion report as a basis for evaluating the effects of

impingement force and contact stress on the probability of forming adhesive bonds between the cell and the substrate.

APPENDIX 1: EVALUATION OF ERRORS FROM APPROXIMATIONS IN THE EQUILIBRIUM EQUATIONS

Force balance on the upstream side of the cell

In deriving Eq. 5 the force balance across the cell boundary not in contact with the bead was taken relative to ambient pressure, that is, the pressure in the suspending fluid in the chamber outside the pipette. Yet, from examination of Fig. 2 *B*, it is apparent that the portion of the cell boundary with radius R_c is actually at equilibrium with the fluid in the pipette just upstream of the cell. The pressure in this region is slightly greater than the pressure in the suspending fluid. Thus, we might more properly write

$$P_i - P_u = \frac{2T_{cort}}{R_c}, \tag{A1}$$

where P_u is the pressure in the pipette immediately upstream of the cell relative to the suspending fluid outside the pipette. This results in a slightly different expression for the equilibrium state,

$$A_{mac} = 2\pi R_b\left(R_b - \sqrt{R_b^2 - \frac{F}{2\pi T_{cort}\left(\frac{1}{R_c}+\frac{1}{R_b}\right) + \pi P_u}}\right). \tag{A2}$$

The magnitude of P_u affects the calculated value of the cortical tension. Its magnitude depends on the impingement pressure applied to the system, and the pressure loss in the pipette due to the leak flow around the cell. An expression for P_u has been derived by Shao and Hochmuth (1996),

$$P_u = \frac{8L_{eq}F}{\pi R_p^3}\left[\frac{2\sqrt{2}}{9\pi}\varepsilon^{5/2} - \frac{8}{9\pi^2}\varepsilon^3 + \cdots O\left(\varepsilon^{7/2}\right)\right]. \tag{A3}$$

Using this expression and the values of ε and L_{eq} for the present study, we estimate that neglecting P_u in Eq. A1 could lead to an overestimation of T_{cort} of ~5% for the data of the present study.

Note that the inclusion (or exclusion) of P_u has no effect on the predictions for the dynamic response of the cell. This is because P_u enters the governing equation for the dynamic process (Eq. 11) in exactly the same combination with T_{cort} as it does in Eq. A2. Thus, inclusion of P_u in the equilibrium analysis results in a slightly lower value of T_{cort}, and this lower value exactly compensates for the inclusion of P_u in the dynamic analysis.

Changes in ε due to cell deformation

It is possible that deformation of the cell when it contacts the bead may affect the width of the gap between the cell and the pipette wall. To determine how much this might affect our calculation of the force, we measured the vertical dimension of the cell before and during contact with the bead. (Although optical diffraction limits the absolute accuracy of these measurements, changes in the cell diameter could be determined more accurately by measuring the displacement of consistently chosen locations within the diffracted image.) The deformation is largest for the largest pressures, and varied from cell to cell. The largest changes in cell diameter were $<0.05\ \mu$m. Although this sometimes resulted in a substantial percentage change in ε, the effect on the calculated value of the force was small because the percentage change was largest when ε was smallest and had the least effect on the calculated force. We estimate that for the largest impingement pressures (where the deformation was greatest) the error in force was typically $<8.5\%$ and ~11% in the worst case. Note that in this case our approximation that ε does not change would result in an underestimation of T_{cort}, thus compensating for errors that might result from neglecting P_u in Eq. A1.

APPENDIX 2: IMPORTANCE OF ENTRANCE EFFECTS IN RADIAL GROWTH MODEL

It is important to consider the possibility of a significant pressure drop occurring within the cell in the vicinity of the impinging bead, which could lead to an overestimation in the calculation of the pressure jump at the cell surface. Since the entrance flow induced by the impinging bead is initially axial in direction, it is appropriate to model this in cylindrical coordinates where the axial coordinate z is parallel to the bead motion, θ is the symmetry direction, and here r is directed radially outward from the z axis (rather than the spherical r-coordinate used earlier). Retaining the relevant noninertial terms in the z-component of the Navier-Stokes equation yields

$$\frac{\partial p}{\partial z} = \mu\frac{\partial^2 v_z}{\partial z^2}. \tag{A4}$$

If the fluid decelerates from a velocity equal to the bead velocity at the cell surface, down to some lower value near the cell center, this would appear to be associated with a negative pressure change of

$$\Delta p \sim -\mu v/R. \tag{A5}$$

Substituting characteristic values from the current study, one finds that this pressure drop is predicted to be of the same order of magnitude as the pressure drop across the interface,

$$\Delta p \sim -\gamma/R. \tag{A6}$$

However, both the entrance flow and the local pressure are functions of both r and z: i.e., $v(r,z)$, $p(r,z)$. As the z-component of the velocity decreases, it is converted to an outwardly-directed radial velocity. Indeed, once the fluid reaches a spherical shell near the center of the cell of equal surface area to the contact area of the bead, the radial velocity component must equal the original z-velocity of the bead due to mass conservation. Now consider the relevant terms in the r-momentum equation,

$$\frac{\partial p}{\partial r} = \mu\frac{\partial^2 v_r}{\partial z^2}. \tag{A7}$$

Since the radial component of the velocity is initially zero at the bead surface and *increases* to a value equal in magnitude to the z-velocity of the bead at a location near the cell center, by scaling arguments we expect a *positive* pressure change associated with this velocity change of magnitude,

$$\Delta p \sim +\mu v/R. \tag{A8}$$

This positive pressure difference will approximately balance the negative pressure change predicted solely from the z-momentum equation. Conceptually, this implies that the z-velocity imparted by the bead on the fluid is efficiently converted to a radial velocity with minimal pressure losses. Thus, based on this dimensional analysis of the governing equations, we predict that there is no significant pressure drop associated with the entrance flow, and that the calculation of the pressure jump at the cell surface based on the micropipette pressure remains valid.

The authors thank Katie Bush and Donna Brooks for assistance with data analysis, and Richard Bauserman for assistance in performing the experiments. We also thank an anonymous reviewer for raising the question of pressure losses in the vicinity of the impinging bead, and suggesting the scaling analysis of Appendix 2.

This work was supported by the U.S. Public Health Service under National Institutes of Health grant HL-18208.

REFERENCES

Alon, R., D. A. Hammer, and T. A. Springer. 1995. Lifetime of the P-selectin-carbohydrate bond and its response to tensile force in hydrodynamic flow. *Nature*. 374:539–542.

Bruehl, R. E., T. A. Springer, and D. F. Bainton. 1996. Quantitation of L-selectin distribution on human leukocyte microvilli by immunogold labeling and electron microscopy. *J. Histochem. Cytochem.* 44:835–844.

Chesla, S. E., P. Selvaraj, and C. Zhu. 1998. Measuring two-dimensional receptor-ligand binding kinetics by micropipette. *Biophys. J.* 75:1553–1572.

Dembo, M., D. C. Torney, K. Saxman, and D. Hammer. 1988. The reaction-limited kinetics of membrane-to-surface adhesion and detachment. *Proc. R. Soc. Lond. B Biol. Sci.* 234:55–83.

Dimitrakopoulos, P., and J. J. L. Higdon. 1998. On the displacement of three-dimensional fluid droplets from solid surfaces in low-Reynolds-number shear flows. *J. Fluid Mech.* 377:189–222.

Dong, C., and R. Skalak. 1992. Leukocyte deformability: finite element modeling of large viscoelastic deformation. *J. Theor. Biol.* 21:173–193.

Dong, C., J. Cao, E. J. Struble, and H. H. Lipowsky. 1999. Mechanics of leukocyte deformation and adhesion to endothelium in shear flow. *Ann. Biomed. Eng.* 27:298–312.

Dong, C., and X. X. Lei. 2000. Biomechanics of cell rolling: shear flow, cell-surface adhesion, and cell deformability. *J. Biomech.* 33:35–43.

Drury, J. L., and M. Dembo. 2001. Aspiration of human neutrophils: effects of shear thinning and cortical dissipation. *Biophys. J.* 81:3166–3177.

Erlandsen, S. L., S. R. Hasslen, and R. D. Nelson. 1993. Detection and spatial distribution of the beta 2 integrin (Mac-1) and L-selectin (LECAM-1) adherence receptors on human neutrophils by high-resolution field emission SEM. *J. Histochem. Cytochem.* 41:327–333.

Evans, E., and B. Kukan. 1984. Passive material behavior of granulocytes based on large deformation and recovery after deformation tests. *Blood.* 64:1028–1035.

Evans, E., and A. Yeung. 1989. Apparent viscosity and cortical tension of blood granulocytes determined by micropipette aspiration. *Biophys. J.* 56:151–160.

Fernandez-Segura, E., J. M. Garcia, and A. Campos. 1996. Topographic distribution of CD18 integrin on human neutrophils as related to shape changes and movement induced by chemotactic peptide and phorbol esters. *Cell. Immunol.* 171:120–125.

Firrell, J. C., and H. H. Lipowsky. 1989. Leukocyte margination and deformation in mesenteric venules of rat. *Am. J. Physiol.* 256:H1667–H1674.

Herant, M., W. A. Marganski, and M. Dembo. 2003. The mechanics of neutrophils: synthetic modeling of three experiments. *Biophys. J.* 84: 3389–3413.

Humphrey, J. A. C., R. L. Hummel, and J. W. Smith. 1974. Note on the mass transfer enhancement due to circulation in growing drops. *Chem. Eng.* 29:1496–1500.

Kern, W. F., and J. R. Bland. 1948. Solid Mensuration with Proofs. Wiley, New York.

Lei, X., M. B. Lawrence, and C. Dong. 1999. Influence of cell deformation on leukocyte rolling adhesion in shear flow. *J. Biomech. Eng.* 121:636–643.

MacLeod, C. A., and C. J. Radke. 1993. A growing drop technique for measuring dynamic interfacial tension. *J. Colloid. Interf. Sci.* 160:435–448.

Needham, D., and R. M. Hochmuth. 1990. Rapid flow of passive neutrophils into a 4-micron pipette and measurement of cytoplasmic viscosity. *J. Biomech. Eng.* 112:269–276.

Needham, D., and R. M. Hochmuth. 1992. A sensitive measure of surface stress in the resting neutrophil. *Biophys. J.* 61:1664–1670.

Ritchie, K., and E. Evans. 1997. Sensitive force technique to probe molecular adhesion and structural linkages at biological interfaces. *Biophys. J.* 72:1541–1555.

Schmid-Schonbein, G. W., K. L. P. Sung, H. Tozeren, R. Skalak, and S. Chien. 1981. Passive mechanical properties of human leukocytes. *Biophys. J.* 36:243–256.

Scriven, L. E. 1960. Dynamics of a fluid interface. *Chem. Eng. Sci.* 12: 98–108.

Shao, J. Y., and R. M. Hochmuth. 1996. Micropipette suction for measuring picoNewton forces of adhesion and tether formation from neutrophil membranes. *Biophys. J.* 71:2892–2901.

Shao, J. Y., H. P. Ting-Beall, and R. M. Hochmuth. 1998. Static and dynamic lengths of neutrophil microvilli. *Proc. Natl. Acad. Sci. USA.* 95:6797–6802.

Spillmann, C. M., E. B. Lomakina, and R. E. Waugh. 2004. Neutrophil adhesive contact dependence on impingement force. *Biophys. J.* 87: 4237–4245.

Spillmann, C., D. Osorio, and R. Waugh. 2002. Integrin activation by divalent ions affects neutrophil homotypic adhesion. *Ann. Biomed. Eng.* 30:1002–1011.

Tees, D. F. J., R. E. Waugh, and D. A. Hammer. 2001. A microcantilever device to assess the effect of force on the lifetime of selectin-carbohydrate bonds. *Biophys. J.* 80:68–82.

Tsai, M. A., R. S. Frank, and R. E. Waugh. 1993. Passive mechanical behavior of human neutrophils-power-law fluid. *Biophys. J.* 65:2078–2088.

Williams, T. E., S. Nagarajan, P. Selvaraj, and C. Zhu. 2001. Quantifying the impact of membrane microtopology on effective two-dimensional affinity. *J. Biol. Chem.* 276:13283–13288.

Yeung, A., and E. Evans. 1989. Cortical shell-liquid core model for passive flow of liquid-like spherical cells into micropipettes. *Biophys. J.* 56:139–149.